LA-UR-95- 2728

CONF-950856--2

Los Alamos National Laboratory is operated by the University of California for the United States Department of Energy under contract W-7405-ENG-36

TITLE: **APPLICATION OF FACETED YIELD SURFACES FOR SIMULATING COMPRESSION TESTS OF TEXTURED MATERIALS**

AUTHOR(S): P(aul) J. Maudlin, T-3
S(tuart) I. Wright, CMS
G(eorge) T. Gray, III, MST-5
J. W. House, Eglin AFB

SUBMITTED TO: *Proceedings of the International Conference on Metallurgical and Materials Applications of Shock-Wave and High-Strain-Rate Phenomena, El Paso, Texas, August 6–10, 1995*

Los Alamos
Los Alamos National Laboratory
Los Alamos, New Mexico 87545

FORM NO. 836 R4
ST. NO. 2629 5/81

Application Of Faceted Yield Surfaces For Simulating Compression Tests Of Textured Materials

P. J. Maudlin[a] , S. I. Wright[a], G. T. Gray III[a], and J. W. House [b]

Constitutive modeling used for most forming calculations assume an isotropic yield function with isotropic hardening. This assumption usually takes the form of an isotropic elastic stiffness tensor, a realistic flow stress model and a von Mises yield function. Real materials deviate from isotropy both in elasticity and plasticity. The calculations described here relax the assumptions of isotropic elasticity and plasticity by utilizing direct measurements of the elastic stiffness tensor and anisotropic representations of yield surfaces, in particular surfaces tessellated from direct measurements of material texture. This effort validates the use of such constitutive modeling by simulating quasi-static, uniaxial stress compression and Taylor Cylinder impact, and comparing their cross-sectional "footprints" to experimental data.

1. INTRODUCTION

Most metallic materials used in high-rate forming are polycrystalline aggregates having a mechanical response that is strongly dependent on dislocation distribution, dislocation interactions with interstitial atoms and other barriers, and a variable crystallographic texture. The elastoplastic constitutive description needed for accurate simulation of high-rate forming must include a strain-rate dependent flow stress model and often some description of the anisotropic yield behavior resulting from the material's texture. A directionally averaged behavior for a given material can be described with a flow stress (σ) model representing the isotropic yield response as a function of work hardening, strain-rate hardening, and thermal softening. Such flow stress models range from simple forms[1] to more complicated path dependent descriptions with internal state variables such as the Mechanical Threshold Stress[2] (MTS) model.

The directionality of yield behavior as determined by grain orientation (texture), grain size, or grain aspect ratio can be described by a anisotropic yield surface shape that can evolve with deformation. If it is assumed that the yield surface shape is dominated by textural effects, this shape can be computed from a polycrystalline average, taken over a range of grain orientations, of the

[a] Los Alamos National Laboratory, Los Alamos, New Mexico 87545

[b] Wright Laboratories, Munitions Directorate, Eglin Air Force Base, Florida

microscopic behavior of constituent grains. It is this type of modeling that is embodied in a polycrystal plasticity code such as LApp[3,4].

The combination of a rate-dependent flow stress model[2] describing isotropic hardening and a tessellated[5] or fitted yield surface form (quadratic[6] or piece-wise[7,8,9,10]) providing a shape, both coupled together in a continuum mechanics code, represents an improved computational capability for simulating forming problems.

2. YIELD SURFACE REPRESENTATION

In general, yield functions can be viewed as five dimensional in terms of deviatoric stress components s_{ij}, i.e.,

$$\left[s_{ij}\right] = \begin{bmatrix} s_{11} & s_{12} & s_{13} \\ s_{12} & s_{22} & s_{23} \\ s_{13} & s_{23} & s_{33} \end{bmatrix} \tag{1}$$

where this tensor has five independent components (recall $s_{kk} = 0$). Therefore the stress components (s_{11}, s_{22}, s_{12}, s_{13}, s_{23}) define the general five-dimensional space that needs to be spanned by some convex yield function, constraining the magnitude of the stress state during plastic flow.

Now consider the 5D case where a set of stress points are generated by repetitive polycrystal probes of a measured material orientation distribution function (ODF). This set of points can be tessellated (a linear fitting complete with associated connectivity) into a piece-wise surface in five space using a tessellation algorithm[6], the whole of which can be mathematically expressed (using indicial notation) as the set:

$$\left\{ f^{\beta} \equiv \alpha_{ij}^{\beta} \tilde{s}_{ij} - \tilde{\sigma}^{\beta} = 0, \beta = 1,2,\ldots,M \right\} \tag{2}$$

The linear functions (say M *hyperplanes)* appearing in Eq. (2) are expressed in normal form that defines the α_{ij}^{β} as coefficients of a vector normal to the hyperplane and $\tilde{\sigma}^{\beta}$ as the minimum distance between the origin and the β hyperplane.

The yield function given by Eq. (2) represents only a normalized yield *shape* and thus needs to be scaled with a flow stress function[11] σ (in equivalent stress units) to obtain the absolute surface (in terms of s_{ij}, σ^{β}) in deviatoric stress space, i.e.,

$$s_{ij} = \tilde{s}_{ij}\, \sigma \frac{1}{M} \qquad \text{and} \qquad \sigma^{\beta} = \tilde{\sigma}^{\beta}\, \sigma \frac{1}{M} \tag{3a, b}$$

where the quantities overscored with a tilde represent normalized variables: the results of tessellated polycrystal calculations. The average Taylor Factor $\overline{M}$ appearing in Eqs. (3) corresponds in direction to that of the uniaxial stress data obtained to characterize the flow stress σ.

Tessellation of a general 5D yield surface from a set of stress points to obtain the coefficients needed for Eq. (2) can be a difficult process. Under the assumption of mirror plane symmetry (orthotropy) and sign independence for the yield surface, Canova, Kocks and Tome[4] have shown that the 5D surface can be decoupled into two closed subspaces of lower dimension: a 2D subspace represented on the π-plane and a 3D shear subspace. The π-plane contains the yield envelope for the normal stress components, and the shear subspace contains the yield envelope for the shears. An example of such a yield surface tessellation is shown in Figs. 1, which is a tantalum (BCC) yield surface corresponding to a uni-directional rolling texture and thus closely approximates an orthotropic mechanical response. Figure 1a presents the π-plane yield surface for Ta being compared to a von Mises circle, and Fig. 1b shows the shear surface; an isotropic von Mises shear response in this subspace would be a sphere. The round symbols in Fig. 1a and the vertices in Fig. 1b are the stress points generated via a polycrystal code[4], probing a discrete Ta ODF with a set of strain increments in the context of a polycrystal calculation.

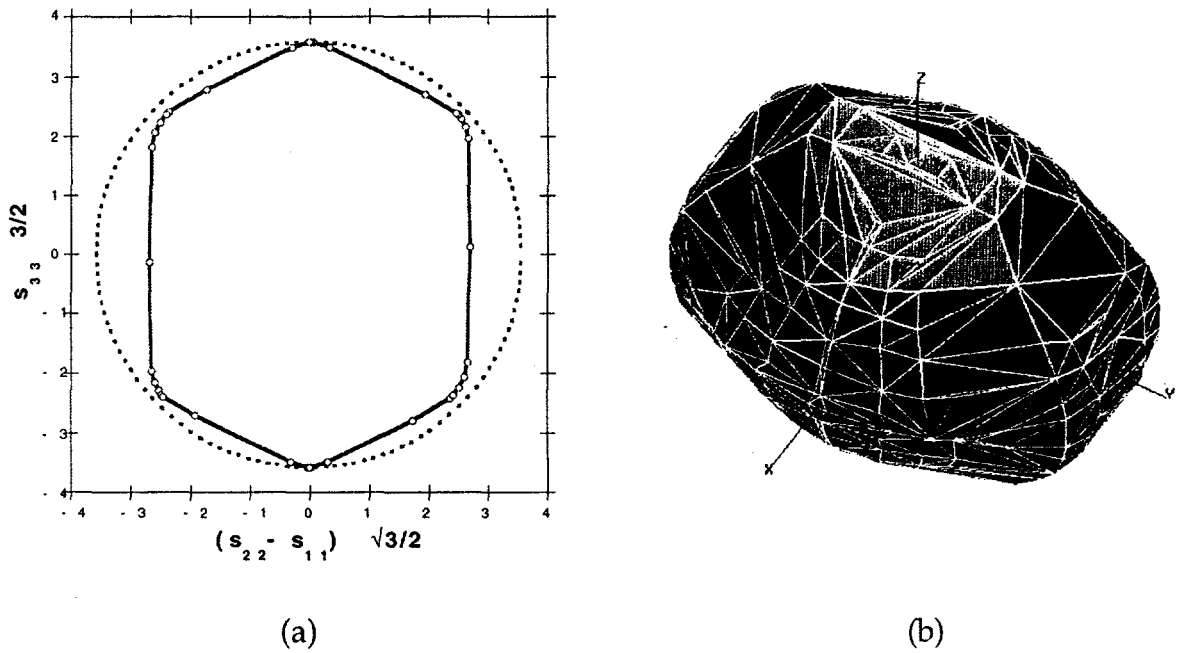

Figure 1: a) Normal subspace (π-plane) comparison of a piece-wise Tantalum yield surface (shown by the solid lines and points) with a von Mises function (dotted curve). b) Shear subspace $\left(x,y,z: \tilde{s}_{12}, \tilde{s}_{13}, \tilde{s}_{23} \right)$ *perspective of a piece-wise Tantalum yield surface. This surface contains 800 stress vertices and 628 planes.*

Under the assumptions of orthotropy and sign-independence, the yield function given by Eq. (2) mathematically decouples into the two sub-functions

$$\left\{ f^{\beta} \equiv \alpha_{11}^{\beta} \tilde{s}_{11} + \alpha_{33}^{\beta} \tilde{s}_{33} - \tilde{\sigma}^{\beta} = 0, \beta = 1,2,\ldots,m \right\} \tag{4a}$$

$$\left\{ f^{\beta} \equiv \zeta_{12}^{\beta} \tilde{s}_{12j} + \zeta_{13}^{\beta} \tilde{s}_{13} + \zeta_{23}^{\beta} \tilde{s}_{23} - \tilde{\sigma}^{\beta} = 0, \beta = 1,2,\ldots,n \right\} \tag{4b}$$

where the linear functions are expressed in normal form defining ζ_{ij}^{β} and α_{ij}^{β} as coefficients of a vector normal to the line or plane, respectively, and σ^{β} as the minimum distance between the stress origin and the β line or plane. The 2D yield function represented by Eq. (4a) and Fig. 1a is basically a linear interpolation of 36 π-plane stress points into 36 lines, and the 3D yield function represented by Eq. (4b) and Fig. 1b is a linear interpolation of 800 shear stress points into 628 planes.

3. MULTISURFACE PLASTICITY THEORY

The set of piece-wise linear functions represented by Eqs. (4) and Figs. 1 were utilized in a three-dimensional continuum mechanics code (EPIC-92[12]) in a multisurface elastoplastic constitutive algorithm[10]. This algorithm is based on the multisurface plasticity theory of Koiter[7] and Simo[8] with modifications that facilitate its use in the constitutive framework of an explicit continuum code whose purpose is high-rate applications. The multisurface plasticity algorithm was described in detail in Ref. 10 for the case of a general 5D yield function; here we only indicate the modifications associated with the orthotropic simplification.

The multisurface plasticity theory follows classical associated flow theory starting with an anisotropic form of Hooke's law, $\dot{s}_{ij} = E_{ijkl}\dot{e}^{e}_{kl}$, written in terms of a deviatoric stress rate and strain rate $\dot{e}_{ij}$ (deviatoric portion of the symmetrical part of the velocity gradient tensor), where E_{ijkl}, is a symmetric elastic constant (stiffness) tensor. Assuming the standard practice of partitioning the strain-rate $\dot{e}_{ij}$ into elastic, $\dot{e}^{e}_{ij}$, and plastic parts, $\dot{e}^{p}_{ij}$, the flow rule for the plastic part is expressed as a summation of contributions from those linear functions[7,8] which are *active:* (hence the subscript "act"):

$$\dot{e}^{p}_{ij} = \sum_{\beta=1}^{M_{act}} \dot{\lambda}^{\beta} \frac{\partial f^{\beta}}{\partial s_{ij}} \tag{5}$$

Here $\dot{\lambda}^{\beta}$ is a time dependent proportionality scalar. Note that the stress gradients in Eq. (5) are just the constants α_{ij}^{β} or ζ_{ij}^{β} since the individual $f^{\beta}(s_{ij})$ functions are linear; thus we have for our particular choice of Eqs. (4):

$$\dot{e}_{ij}^{p} = \delta_{ij} \sum_{\beta=1}^{m_{act}} \dot{\lambda}^{\beta} \alpha_{ij}^{\beta} + \left(1 - \delta_{ij}\right) \sum_{\beta=1}^{n_{act}} \dot{\lambda}^{\beta} \varsigma_{ij}^{\beta} \quad , \text{no } \Sigma \tag{6}$$

where δ_{ij} is the Kronecker delta function.

The next step is the standard enforcement of yield surface consistency by taking the time derivative of Eqs. (4) and substituting for the stress rate and the plastic strain rate using Hooke's law and Eq. (6), respectively. This process is straightforward associative flow treatment that results in a system of $(m_{act} + n_{act})$ linear equations for $(m_{act} + n_{act})$ unknowns $\dot{\lambda}^{\beta}$'s. The mathematical advantage of using the orthotropic and sign-independence assumptions is the decoupling of the normal and shear equation sets: The use of the general yield function given by Eq. (2) results in a set of M_{act} (where $M_{act} = m_{act} + n_{act}$) coupled linear equations, whereas the use of the orthotropic yield functions given by Eqs. (4) results in two uncoupled systems of equations (m_{act} and n_{act}, respectively) that can be solved independently.

As might be anticipated, most of the work associated with the use of this algorithm involves identifying the active linear functions (m_{act}, n_{act}) out of a total population of functions (m,n) that can be made arbitrarily large for numerical accuracy. The logic for discriminating the active linear functions is discussed in some detail in Ref. 10.

4. RESULTS: UNIAXIAL COMPRESSION TESTS AND TAYLOR CYLINDER TESTS

Consider a plate of tantalum having a right-handed *material* coordinate system (axes 1', 2', 3') where the 3' axis is thru-thickness and the 1' and 2' axes are both in plane; it is in such a coordinate system that the stresses of Figs. 1 are cast. This tantalum plate was subjected to a cross-rolling process that produces an orthotropic material texture. A cylindrical compression specimen was cut from this plate for a so-called in-plane (IP) orientation (the axis of the cylindrical specimen is parallel to the 1' or 2' direction). Consider also a fixed laboratory reference frame (axes x, y, z) representing the principle axes of the uniaxial compression such that for the IP specimen the loading is applied along the laboratory z-axis (cylindrical specimen centerline) that is identical to the material 2'-axis, and the y-axis is identical to the 3'-axis. The Fig. 1a π-plane yield function indicates that the 3' direction is the "hard" direction, since the distance between the stress origin and the yield function is at a maximum, and the 1' or 2' directions are "weaker."

A uniaxial compression test was simulated with the explicit, finite-element EPIC92 code using the orthotropic elastoplastic modeling discussed above and in Ref. 10. Since the test was quasi-static, the strain-rate and thermal dependencies of the used flow stress model were constrained to 10^{-3} s^{-1} and room temperature, respectively. The specimen (L/D = 1.196, L = 7.615 mm) was spatially modeled

with about 5200 tetrahedral elements. The specimen was loaded uniaxially between two elastic tool steel platens. Since an explicit, time-dependent code cannot economically simulate the specimen deformation quasi-statically, the platens were accelerated from zero to 100 m/s until the experimentally measured axial displacement (3.307 mm) was achieved; stress wave effects were thus minimized.

Figure 2a presents a computed final IP specimen geometry compressed to a axial true strain of -77%. The specimen's footprint is elliptic with a calculated eccentricity (ratio of major to minor axes) of 1.33. Superimposed on the calculated footprint is the experimental result (digitized footprint interface) that has an eccentricity of 1.34; the experimental footprint matches closely the calculated result in the y (3') direction, and is slightly larger in the x (1') direction.

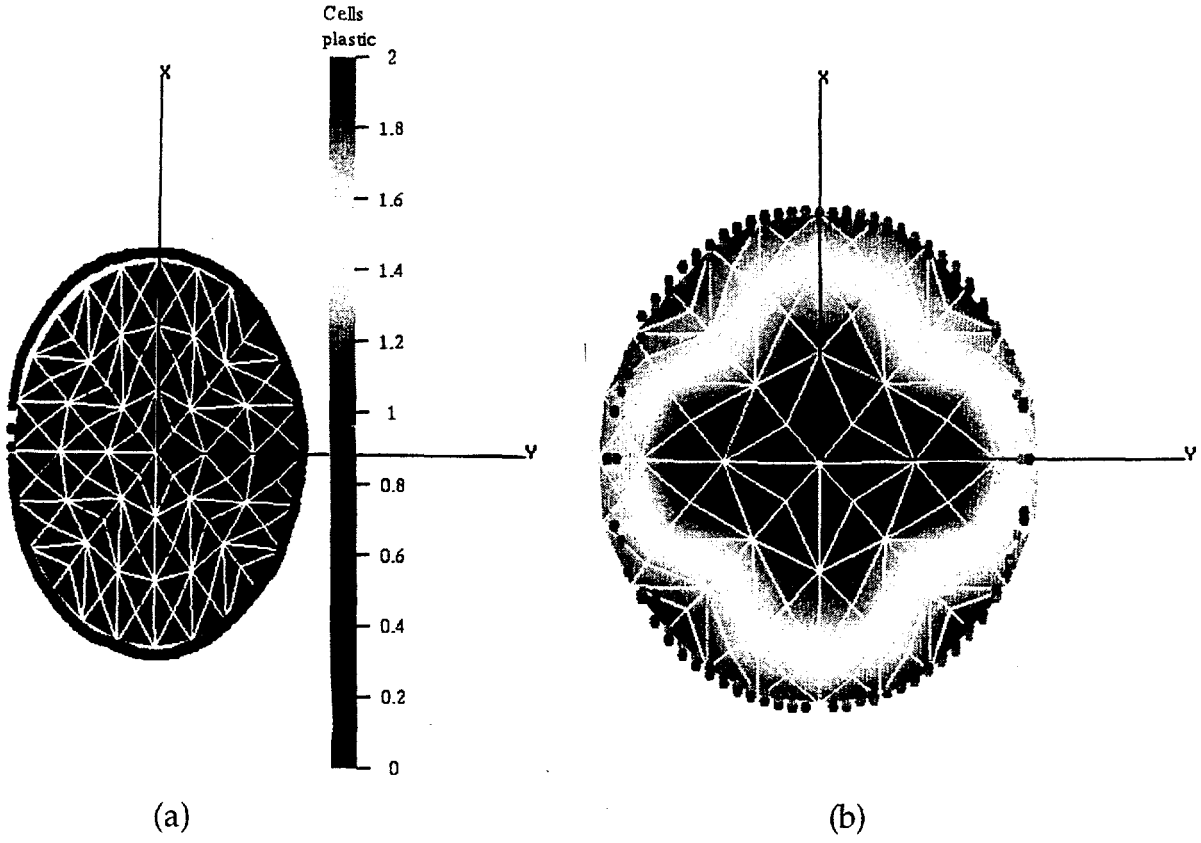

(a) (b)

Figure 2: Comparison of a (a) uniaxial stress compression (b) Taylor Cylinder simulation results showing the cylinder footprint at late-times with experimental footprint from three tests. The tantalum elastic stiffness tensor given in Ref. 10, the yield functions shown in Figs. 1, a Mie-Gruniesen equation-of-state, and the MTS flow stress model given in Ref. 11 (characterized for the this Ta) were used in the simulations. The material axes for the initial cylinder are rotated 90° (in the 1' - 3' plane) from the laboratory impact axes.

A Taylor Cylinder test series was conducted that consisted of three shots using tantalum 30 caliber (7.62 mm diameter) cylinders 1.5-inch long (38.1 mm). The cylinders were launched using powder gun propellant from a caliber 30 Mann barrel. The velocity of the projectiles was measured by both pressure transducers and parallel laser beams crossing the flight path. Velocities determined from the two systems were about 175 m/s, agreeing to within +/- 3.0 m/s. The target was constructed of 4340 steel heat treated to a surface hardness of Rc 58. After testing, geometric data of the deformed specimen was generated using an optical comparitor. The data consist of three digitized footprints that define the cross-sectional area at the impact interface, and are shown as points in Fig. 2b.

The Taylor cylinders were initially cut from the same Ta plate in the same orientation as discussed above for the compression specimens. Assuming isotropic strength (or even anisotropic strength with transverse isotropy), a Taylor impact event is normally an axisymmetric problem that can be simulated with a continuum code with two space dimensions. However, with the introduction of a directionally dependent constitutive description using an orthotropic yield surface, the Taylor problem will develop a three-dimensional deformation distribution that needs to be simulated in three dimensional space.

The Taylor Cylinder tests were simulated with the EPIC-92 code using the orthotropic yield functions of Figs. 1. The simulated impact results are shown in Fig. 2b in terms of late-time cylindrical footprints at the impact interface and compare well with the experimental data. The elliptical footprint shown in Fig. 2b has an eccentricity of 1.15 that compares to 1.17 for the experimental footprints; for isotropy the footprint would be round with an eccentricity of 1.

5. CONCLUSIONS

A faceted, two-subspace yield function representation for rolled orthotropic tantalum was successfully used as the constitutive description in three dimensional simulations of uniaxial stress compression tests and Taylor Cylinder tests. These calculational results were in good agreement with the experimental footprint data. It should be noted that the material texture in these simulations was assumed to be constant with respect to material deformation, where in reality some texture evolution certainly would have occurred, changing the shape of the Figs. 1 yield functions. The good agreement between simulations and experiments indicates that the texture evolution was small for these specific problems.

ACKNOWLEDGMENT

The efforts of Edwin M. Privette in reducing the experimental Taylor Cylinder footprint data were very much appreciated, and were supported by the Armament Directorate of Wright Laboratories, USAF. This work was made possible by the Joint DoD/DOE Munitions Technology Development Program.

REFERENCES

1. G. R. Johnson and W. H. Cook, Proceed. 7th Inter. Sym. on Ballistics, The Hague, The Netherlands, April 1983.
2. P. S. Follansbee and U. F. Kocks, Acta Metall., 36, No. 1, 81–93 (1988).
3. G. R. Canova, U. F. Kocks and C. N. Tome, J. *Mech. Phys. Solids*, 33, 371–397 (1985).
4. A. D. Rollett, D. Juul Jensen and M. G. Stout, Proc. 13th Risø International Symposium on Materials Science: *Modeling of Plastic Deformation and Its Engineering Applications*, Editors: S. I. Anderson, J. B. Bilde Sørenson, N. Hansen, D. Juul Jensen, T. Leffers, H. Lilholt, T. Lorentzen, O. B. Pedersen and B. Ralph, Risø National Laboratory, Roskilde, Denmark, pp. 93-109 (1992).
5. M. S. Sahota, *Proceed. Next Free-Lagrange Conf.*, Moran, Wyoming, 3–7 June, 1990.
6. R. Hill, The Mathematical Theory of Plasticity, Oxford University Press, London, 1950.
7. W. T. Koiter, *Quart. Appl. Math.*, 11, 350-354 (1953).
8. J. C. Simo, J. G. Kennedy and S. Govindjee, *Int. J. Num. Methods Engr.*, 26, 2161–2185 (1988).
9. P. J. Maudlin and S. K. Schiferl, *Computer Methods in Applied Mechanics and Engineering* (accepted for publication, June 1995).
10. P. J. Maudlin, S. I. Wright, U. F. Kocks and M. S. Sahota, *Acta Metall* (submitted for publication, March 1995).
11. S. R. Chen and G. T. Gray III, *Proceed. Int. Conf. on Tungsten and Refractory Metals*, McLean, Virginia, 17-19 October, 1994.
12. G. R. Johnson and R. A. Stryk, Air Force Armament Laboratory, Eglin Air Force Base report, AFATL-TR-86-51 (August 1986).

DISCLAIMER